JOURNAL OF GEOPHYSICAL RESEARCH: EARTH SURFACE, VOL. 118, 1161–1176, doi:10.1002/jgrf.20053, 2013

Experimental study on coarse grain saltation dynamics in bedrock channels

Phairot Chatanantavet,[1] Kelin X. Whipple,[2] Mark A. Adams,[2] and Michael P. Lamb[1]

Received 24 April 2012; revised 24 February 2013; accepted 1 March 2013; published 24 June 2013.

[1] Saltation of bed load particles on bedrock surfaces is important for landscape evolution and bedrock incision in steep landscapes. However, few studies have investigated saltation in bedrock channels where, unlike alluvial channels, the bed roughness height and the sediment size may be independent. To address this data gap, we measured the saltation hop height, hop length, and velocity of gravel saltating over a planar bed using 80–160 readings from high-speed photography and direct measurements. Two separate dimensional analyses are used: one leading to a bed shear stress scaling and another leading to a Froude number (*Fr*) scaling. Our new saltation data coupled with numerous data from previous studies suggest that both shear stress and *Fr*-scaling analyses are valid in characterizing bed load saltation dynamics with bed roughness ranging from smooth to alluvial beds. However, the *Fr* approach has the advantages that (1) there is no need to estimate a critical Shields stress $\left(\tau_c^*\right)$, which alone can vary up to 2 orders of magnitude (e.g., 0.001–0.1) due to changes in relative bed roughness and slope and (2) the *Fr*-based scaling fits the saltation data set better in a least squares sense. Results show that the saltation velocity of bed load is independent of grain density and grain size and is linearly proportional to flow velocity. Saltation height has a nonlinear dependence on grain size. Saltation length increases primarily with flow velocity, and it is inversely proportional to submerged specific density. Our results suggest that either τ_c^* or bed roughness coefficient must be properly estimated to yield accurate results in saltation-abrasion models.

Citation: Chatanantavet, P., K. X. Whipple, M. Adams, and M. P. Lamb (2013), Experimental study on coarse grain saltation dynamics in bedrock channels, *J. Geophys. Res. Earth Surf.*, *118*, 1161–1176, doi:10.1002/jgrf.20053.

1. Introduction

[2] The mechanics of sediment transport are fundamental to hydrology, geology, oceanography, and civil engineering. Transport of particles in water can be classified into four modes: rolling, sliding, saltating, and suspended motion [*Bagnold*, 1966]. The type of transport depends on hydraulic conditions, channel bed surface, particle shape, grain density, and grain size. Among these modes of transport, saltation is the dominant mode of bed load transport [*Hu and Hui*, 1996; *Ancey et al*., 2008] and plays a key role in bedrock channel incision by bed load abrasion [e.g., *Sklar and Dietrich*, 2004; *Chatanantavet and Parker*, 2009; *Lamb et al*., 2008a; *Johnson and Whipple*, 2010]. Nonetheless, saltation has been studied almost exclusively under conditions common in alluvial channels. Our interest is in the role of saltation dynamics in controlling river incision by abrasion in steep bedrock rivers, which typically have hydraulic and channel bed conditions under which saltation has not been studied.

[3] Grain saltation has been studied since the early work by *Gilbert* [1914]. *Einstein* [1950] conducted a flume study and found that the saltation length is a function of particle size, shape, and flow characteristics. *Bagnold* [1966] found that the bed load movement seems to be dominated by the gravity force and not significantly affected by turbulent eddies. However, the role of turbulence in bed load transport has been studied in more detail since then [e.g., *Browand and Ho*, 1983; *Diplas et al*., 2008], and it is indeed important. Several researchers investigated grain saltation in water using high-speed photography from which grain characteristics such as the trajectory height and length as well as the mean particle velocity were determined and analyzed [e.g., *Fernandez Luque and van Beek*, 1976; *Abbott and Francis*, 1977; *Lee and Hsu*, 1994; *Nino et al*., 1994; *Hu and Hui*, 1996; *Ancey et al*., 2006]. *van Rijn* [1984] utilized the particle saltation characteristics to derive a bed load transport formula. *Wiberg and Smith* [1985] developed a mathematical model that describes the trajectory of a saltating grain. *Sklar and Dietrich* [2004] developed an excess Shields stress–based, nondimensional scaling analysis of published grain saltation trajectory data in their formulation of bedrock abrasion by bed load.

[4] Most previous studies focused on grain saltation (1) over a mobile alluvial bed or a bed with some roughness

[1]Division of Geological and Planetary Sciences, California Institute of Technology, Pasadena, California, USA.
[2]School of Earth and Space Exploration, Arizona State University, Tempe, Arizona, USA.

Corresponding author: P. Chatanantavet, Division of Geological and Planetary Sciences, California Institute of Technology, 1200 E. California Blvd., MC 170-25, Pasadena, CA, USA. (phairot@caltech.edu)

2169-9003/13/10.1002/jgrf.20053

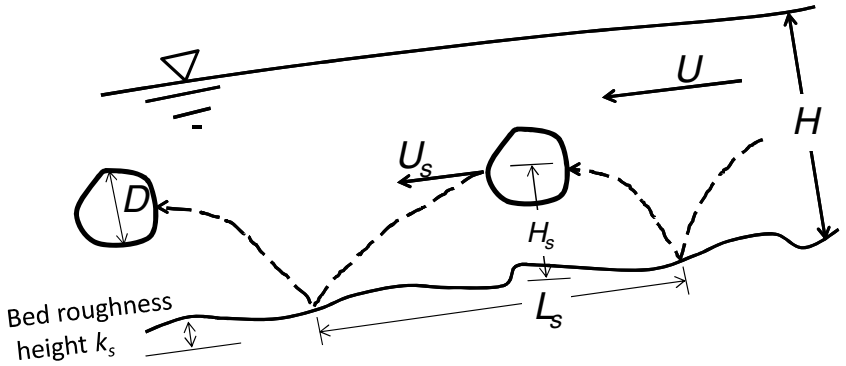

Figure 1. Schematics of saltation mechanics of a coarse particle over a bedrock surface. D is mean grain diameter, k_s is average bed roughness height, U_s is grain saltation velocity, H_s is saltation height, L_s is saltation length, U is averaged flow velocity, and H is water depth.

created by fixing grains onto the bed and (2) under mild slopes (i.e., $S < 0.02$, where S is channel bed slope) and subcritical flow ($Fr < 1$, where Fr is the Froude number), conditions consistent with low-slope, alluvial rivers. *Nino et al*. [1994] and *Ancey et al*. [2006, 2008] are among the few who studied saltation dynamics in high-slope channels ($0.03 < S < 0.10$), again with mobile alluvial beds. While previous work is useful for steep gravel bedded alluvial rivers, it may not be applicable to bedrock rivers, where the river bed has a high coefficient of restitution and can have local bed roughness potentially much smaller or larger than that of an alluvial bed. *Hu and Hui* [1996] investigated grain saltation characteristics over both a rough bed and a smooth plane bed, but only on very mild bed slopes ($S \leq 0.005$) not common in actively incising bedrock channels. Channel slope has been demonstrated to be an important parameter in mountain streams to characterize and categorize channel bed morphologies [e.g., *Montgomery and Buffington*, 1997; *Wohl and Merritt*, 2001]. Additionally, several studies [e.g., *Neill*, 1968; *Buffington and Montgomery*, 1999; *Shvidchenko and Pender*, 2000; *Shvidchenko et al*., 2001; *Mueller et al*., 2005; *Lamb et al*., 2008b] have shown that slope strongly affects the incipient motion of sediment. *Lamb et al*. [2008b] suggested that incipient motion is a function of relative flow roughness (D/H, where D is grain diameter and H is flow depth), which covaries with slope. *Recking* [2009] presented theoretical development of these effects on bed load incipient motion on an alluvial bed, and *Ferguson* [2012] explained this slope dependency as a result of increasing bulk flow resistance. We infer that channel slope (and associated flow velocity and Fr) may likewise influence grain saltation dynamics.

[5] *Chatanantavet* [2007] argued that the saltation characteristics of grains over smooth beds ($D/k_s >> 1$, where k_s is characteristic bed roughness length scale) may differ from those over alluvial beds. He found that a shear stress–based formula for grain saltation velocity based on rough bed data [e.g., *Sklar and Dietrich*, 2004] underestimated the saltation velocity in high-slope (S 0.02), smooth bedrock channels. However, throughout Chatanantavet's analysis, a critical Shields stress of 0.03 was used. It is possible that for relatively smooth bedrock surfaces the critical Shields stress can be much lower than that for alluvial beds [*Wiberg and Smith*, 1985; *Hodge et al*., 2011], which could explain the apparent discrepancy between observed saltation velocity in his flume experiments and predictions based on *Sklar and Dietrich* [2004]. *Hodge et al*. [2011] used a force balance model by *Kirchner et al*. [1990] and found that on smooth bedrock beds the critical Shields stress could be 1–2 orders of magnitude lower than on alluvial beds. However, they also estimated the critical Shields stress to be 0.038 for the Calder River, a value similar to alluvial rivers, despite about 80% bedrock exposure.

[6] In this paper, we extend the analysis of saltation trajectories in *Sklar and Dietrich* [2004] by combining new and published data and developing two empirical scaling analyses (shear stress–based and Fr-based) for grain saltation dynamics, specifically grain saltation velocity U_s, saltation length L_s, and saltation height H_s, over various degrees of bed roughness, ranging from a completely smooth planar bed to a fully alluvial (and mobile) bed.

2. Dimensional Considerations

[7] Before presenting and discussing the experimental results, it is useful to introduce fluid flow and particle parameters involved in the saltation process over bedrock or mixed bedrock-alluvial beds. Consider a coarse grain ($D > 2$ mm), with submerged specific density of R ($R = (\rho_s - \rho)/\rho$ where ρ_s and ρ are the densities of sediment and water, respectively), saltating in moving water of average flow depth H and average flow velocity U, over a bed with an average bed roughness height k_s (i.e., standard deviation of the bed elevations) (Figure 1). Variables characterizing the saltation dynamics can be written as a function of other independent dimensional variables involved as follows.

$$U_s, H_s, L_s = f(U, H, S, D, g, k_s, v, R) \tag{1}$$

where g is gravitational acceleration and v is kinematic viscosity of the fluid. Note that only two of U, H, and S are needed since the other one may be calculated from a hydraulic roughness formula (e.g., Manning's equation) if the other two variables and bed roughness (k_s) are known.

In previous work, some researchers have used shear stress as the independent hydraulic variable and some have used flow velocity [e.g., *Schoklitsch*, 1962; *Bathurst*, 1987; *Aguirre-Pe et al*., 2003]. We will demonstrate here that they are equally valid, but each one may have advantages over the other in certain aspects.

2.1. Shear Stress Scaling

[8] For the first dimensional analysis, U is deselected (since only two of U, H, and S are needed) and D is chosen to be a controlling length scale together with g as a scaling parameter. Using the Buckingham Pi theorem for dimensional analysis [*Buckingham*, 1915], one obtains

$$\frac{U_s}{\sqrt{RgD}}, \frac{H_s}{D}, \frac{L_s}{D} = f\left(\frac{H}{D}, S, \frac{k_s}{D}, Re_p, R\right) \tag{2}$$

where Re_p is particle Reynolds number $\left(=\frac{\sqrt{RgD}D}{\nu}\right)$. Then by combining variables, this set of independent dimensionless variables can be rewritten more conventionally as

$$\frac{U_s}{\sqrt{RgD}}, \frac{H_s}{D}, \frac{L_s}{D} = f\left(\tau^*, \frac{H}{D} \text{or } S, \frac{k_s}{D}, Re_p, R\right) \tag{3}$$

where dimensionless bed shear stress or Shields number is $\tau^* = \frac{HS}{RD}$ (for normal flow). Re_p is not important for coarse grains with turbulent wakes [e.g., *Wiberg and Smith*, 1985]. S and H/D are found to be equally valid [e.g., *Lamb et al*., 2008b; *Recking*, 2009], theoretically due to the multiplications leading to τ^* from the Buckingham Pi theorem's rule (retaining only one). Therefore, one can reduce equation (3) to four dominant independent variables as

$$\frac{U_s}{\sqrt{RgD}}, \frac{H_s}{D}, \frac{L_s}{D} = f\left(\tau^*, S \text{ or } \frac{H}{D}, \frac{k_s}{D}, R\right). \tag{4}$$

[9] Furthermore, equation (4) can be rewritten as a set of two equations as

$$\frac{U_s}{\sqrt{RgD}}, \frac{H_s}{D}, \frac{L_s}{D} = f\left(\tau^*, \tau_c^*\right) \tag{5.1}$$

and

$$\tau_c^* = f\left(S, \frac{k_s}{D}, R\right) \tag{5.2}$$

where τ_c^* is the critical value of τ^* at incipient sediment motion. It is important to note the difference between relative physical bed roughness k_s/D (of all types of beds including bedrock) and relative hydraulic roughness H/D. The critical Shields stress has been found to be a strong function of bed slope [*Lamb et al*., 2008b] and the relative bed roughness k_s/D [*Kirchner et al*., 1990; *Buffington et al*., 1992; *Turowski et al*., 2011]. In alluvial beds, k_s is typically taken by $k_s = \alpha D$ where α = 1.5–3 [e.g., *Kamphuis*, 1974; *Parker*, 2004]. In bedrock beds, the standard deviation of local bed elevations could be used to characterize the bed roughness (k_s) since it directly represents the physical roughness of the bed [e.g., *Aberle and Smart*, 2003; *Finnegan et al*., 2007; *Johnson and Whipple*, 2007; *Hodge et al*., 2011]. The dependency of τ_c^* on R (equation (5.2)) has been demonstrated at least recently by *Prancevic et al*. [2012]. Equation (5.1) has been traditionally used in saltation studies [e.g., *Hu and Hui*, 1996; *Sklar and Dietrich*, 2004]. For example, *Sklar and Dietrich* [2004] used mostly saltation data from alluvial beds and found the forms of equation (5.1) to be

$$\frac{U_s}{(RgD)^{1/2}} = 1.56\left(\frac{\tau^*}{\tau_c^*} - 1\right)^{0.56} \tag{6.1}$$

$$\frac{L_s}{D} = 8.0\left(\tau^*/\tau_c^* - 1\right)^{0.88} \tag{6.2}$$

$$\frac{H_s}{D} = 1.44\left(\frac{\tau^*}{\tau_c^*} - 1\right)^{0.50}. \tag{6.3}$$

[10] Note that equation (6.2) is the version presented by *Sklar and Dietrich* [2004] without modification for particle suspension, as suggested by *Lamb et al*. [2008a]. These formulas will be tested against a new compilation of data in section 4.

2.2. Froude Number Scaling

[11] For the second dimensional analysis, from equation (1), again only two of U, H, and S are needed. In this case, S is deselected and H is chosen to be a controlling length scale together with g as a scaling parameter. This leads to five independent dimensionless parameters that are equivalent to equation (2)

$$\frac{U_s}{\sqrt{gH}}, \frac{H_s}{H}, \frac{L_s}{H} = f\left(\frac{U}{\sqrt{gH}}, \frac{D}{H}, \frac{k_s}{H}, Re, R\right) \tag{7}$$

where Re is the flow Reynolds number $\left(Re = \frac{UH}{\nu}\right)$. For turbulent flows in natural rivers, the dependence on Re can be neglected [e.g., *Keulegan*, 1938], and so one finds

$$\frac{U_s}{\sqrt{gH}}, \frac{H_s}{H}, \frac{L_s}{H} = f\left(Fr, \frac{D}{H}, \frac{k_s}{H}, R\right) = f\left(Fr, \frac{H}{D}, \frac{k_s}{D}, R\right) \tag{8}$$

where $Fr = U/\sqrt{gH}$ is the Froude number. Equation (8) is basically the same as equation (4) for the shear stress scaling except instead of τ*; here we have Froude number.

[12] Just as with Re, the fact that some dimensionless parameters are derived and remain in the formal scaling analysis does not necessarily mean that they are important for the system in question (in our case; bed load saltation dynamics). In section 4, we will show that for characterizing all saltation parameters (U_s, L_s, and H_s) using Fr-based scaling, the dimensionless ratio k_s/D (relative bed roughness) does not emerge as an important parameter despite the fact that k_s/D varies considerably from ≈1–3 for alluvial beds with uniform grains, to a much smaller value in experiments with a Plexiglas bed ($k_s/D \sim 10^{-6}$). This is likely because the Fr-based formulas depend on flow velocity, and the bed roughness height (k_s) influences turbulent flow velocity as expressed in the flow resistance equations such as *Keulegan* [1938], *Bathurst* [1985], or other Manning's type equations.

[13] It will be shown in section 4 that equations (5) and (8) are both valid scaling analyses for characterizing bed load saltation dynamics over different bed roughnesses ranging

Table 1. Hydraulic Conditions Within the Test Section (Middle 2 m; see Appendix A)

Run	S	Q_w (l/s)	H (m)	τ_b (N/m^2)[a]	U (m/s)[a]	Fr average[a]	D (mm)	Measurements
1	0.005	86	0.128–0.134	1.50	1.46–1.54	1.32	6.7	U_s, L_s, H_s
2	0.01	35	0.055–0.062	1.21	1.26–1.48	1.77	6.7, 13.4, 25	U_s, L_s, H_s
3	0.02	18.8	0.027–0.032	1.10	1.30–1.56	2.64	6.7	U_s
4	0.03	13	0.017–0.021	1.35	1.36–1.68	3.52	6.7	U_s
5	0.03	69	0.073–0.085	3.53	1.80–2.10	2.22	6.7	U_s
6	0.05	46	0.044–0.053	3.83	1.93–2.35	3.12	6.7	U_s
7	0.07	39	0.032- 0.040	3.72	2.14–2.66	4.04	6.7	U_s
8	0.09	30	0.023–0.028	4.21	2.37–2.93	5.30	6.7, 13.4, 25	U_s, L_s, H_s
9	0.03	35	0.040–0.048	1.82	1.62–1.94	2.71	6.7, 13.4, 25	U_s, L_s, H_s
10	0.05	35	0.034–0.042	3.03	1.87–2.29	3.40	6.7, 13.4, 25	U_s, L_s, H_s

[a]Calculated values. Slope (S), water discharge (Q_w), flow depth (H), and grain diameter (D) are measured values. The rest are calculated values. The ranges in H and U are due to flow acceleration. See Appendix A for detail.

from smooth planar beds to alluvial beds although they both have their advantages in different aspects.

3. Experimental Procedure

3.1. Methods Quantifying Saltation Trajectories

[14] The experimental work was conducted in the Experimental Geomorphology Laboratory at Arizona State University (ASU). The facility consists of a flume with a length of 5 m, a width of 0.45 m, and a depth of 0.45 m. The flume slope can be varied between 0 and 10.0%. The bulk of the experiments involved three different sizes of natural quartzite gravel with mean diameters (and standard deviations σ) of 6.7 $\pm$ 1.0, 13.4 $\pm$ 2.2, and 25.0 $\pm$ 3.2 mm. For $D = 6.7$ mm, we performed separate experiments with both angular and subrounded grains. For $D = 13.4$ mm, the grains were subrounded, and for $D = 25$ mm, the grains were spherical. The associated experimental conditions are shown in Table 1. All experiments were conducted under supercritical flow conditions ($Fr > 1$) to complement existing saltation data from the literature that is exclusively for subcritical flow ($Fr < 1$). The experiments were carried using a smooth Plexiglas bed to complement the majority of previous studies on mobile alluvial beds [e.g., *Nino et al*., 1994; *Ancey et al*., 2006, 2008] and fixed alluvial beds [e.g., *Lee and Hsu*, 1994; *Hu and Hui*, 1996].

[15] The smooth Plexiglas bed, supercritical flow, and imposed boundary conditions complicated our analysis in that spatial flow acceleration persisted over the length of the flume (see Appendix A). The familiar depth-slope product quantifying bed shear stress, $\tau_b = \rho g R_b S$, where R_b denotes the hydraulic radius is valid only for steady, uniform flow and could not be used as an effective measure of bed shear stress in our experiments. Accordingly, local bed shear stress values were estimated from backwater flow modeling, calibrated to experimental measurements of flow depth and, in cases, Reynolds stress (Appendix A). These calculated values of local bed stress are listed in Table 1. The water depth was measured using a ruler (with uncertainty of ~1 mm), and the depth-averaged flow velocity was estimated by dividing water discharge per unit width by flow depth, where the water discharge (Q_w) was measured with approximately 5% uncertainty from a flow meter attached to the flume operating system.

[16] A high-speed camera (Casio High-Speed Exilim EX-FC100) with 420 frames per second was used to record grain saltation trajectories from the transparent sidewall of the ASU flume (Figure 2). Grains were dropped into the flow from above one at a time at the location 1.25 m upstream from the upstream edge of the observing window and generally contacted the bed within 15 cm of the drop point. Grains were observed by eye to travel close to the centerline of the channel, where wall effects are minimal. Saltation height and length were measured from the high-speed videos frame by frame using VLC Media Player. About 80–160 readings of complete trajectories from the high-speed camera were used to calculate each mean value of H_s and L_s. The observation window, located at 3.0 m from the flume's upstream end, had a frame-viewing length of 0.50 m, which typically framed about 2–6 hops of each grain (Figure 2). The saltation velocity for each grain was determined by dividing the traveling distance of 3 m (starting at $x = 1.75$ m from the upstream end, where x is longitudinal distance) by the particle travel time using a stopwatch, using approximately 80 repeat measurements. This method of quantifying U_s was compared with select measurements using the high-speed camera directly resulting in good agreement (within $\pm$12%); consequently, the easier method using a stopwatch was chosen. Note that under these high Fr flows and smooth plane bed condition, no grains ever came to rest during saltation (and that this may be unlikely unless alluvial patches form, which likely occur in lower slope channels ($S < 0.005$) as shown in *Chatanantavet and Parker* [2008]).

3.2. Estimation of the Critical Shields Stress on a Smooth Bed

[17] Previous saltation trajectory equations (e.g., equation (6)) show a dependency on the critical Shields stress $\left(\tau_c^*\right)$, which in turn is a strong function of the local particle friction angle [e.g., *Wiberg and Smith*, 1985]. To estimate critical Shields stresses for our particles on a Plexiglas bed, we used a model for τ_c^* and performed tilt table experiments to measure the particle friction angle following *Buffington et al*. [1992]. Five gravel grains were placed on the table at a time. The table tilt angle was then increased slowly, and the angle was recorded when each grain moved down the slope. This procedure was repeated for 400 grains for two grain sizes (6.7 and 13.4 mm) of subrounded gravel. For these tilt table experiments, the friction angle had an average value of 26° $\pm$ 4° (1σ), which is small compared to the typical friction angle for alluvial beds (~ 60°) [*Buffington et al*., 1992]. This suggests that bed load transport over a

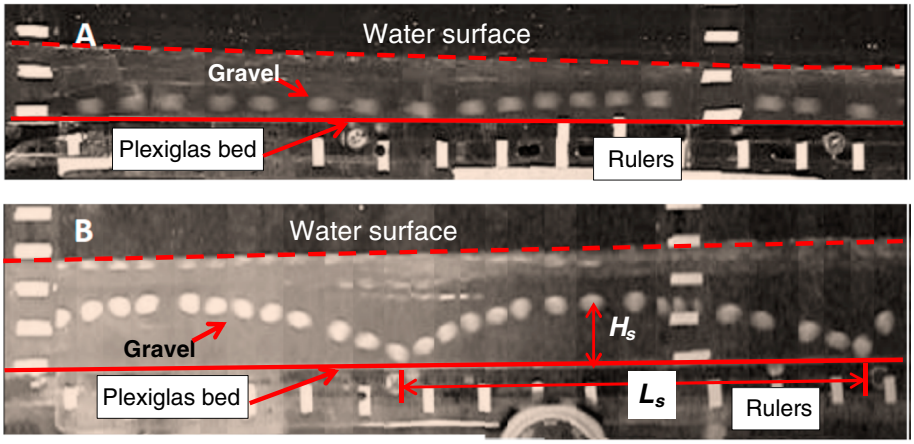

Figure 2. Examples of saltation hops with $D = 6.7$ mm using two different hydraulic conditions: (a) run 8 and (b) run 2 from the high-speed camera. Note that the 6.7 mm grains are not suspended even moving under a very high Fr number flow condition ($Fr = 5.3$ in Figure 2a and $Fr = 1.77$ in Figure 2b). Unlike sediment transport in alluvial bed channels, the bed load grains over smooth plane bed never come to rest on the steep channel here. Flow from left to right. The width of the field of view is about 50 cm.

smooth planar bed is characterized by a much smaller critical Shields stress than for an alluvial bed [e.g., *Hodge et al*., 2011].

[18] In order to estimate τ_c^* for a planar bed to first order, one can consider equation (9) in *Lamb et al*. [2008b] (similar to *Wiberg and Smith* [1985]):

$$\tau_c^* = \frac{2}{C_D}\frac{u_*^2}{\langle u^2\rangle} cos\beta \left(\frac{\tan\phi_0 - \tan\beta}{1 + \left(\frac{F_L}{F_D}\right)\tan\varphi_0}\right)\left(\frac{V_p}{A_{xs}D}\frac{1}{R}\left(\frac{\rho_s}{\rho} - \frac{V_{ps}}{V_p}\right)\right) \tag{9.1}$$

where C_D is drag coefficient, A_{xs} is the cross-sectional area of the particle that is perpendicular to and exposed to the flow, $\langle u^2\rangle$ is local velocity square and spatially averaged over A_{xs}, β is bed slope angle, ϕ_0 is friction angle, F_L is the lift force, F_D is the drag force, V_p is the total volume of the particle, and V_{ps} is the submerged volume of particle. To compare τ_c^* of an alluvial bed $\left(\tau_{c-alluvial}^*\right)$ to a smooth Plexiglas bed $\left(\tau_{c-Plexiglas}^*\right)$, equation (9.1) can be rewritten as

$$\tau_{c-\mathrm{Plexiglas}}^* = \tau_{c-\mathrm{alluvial}}^* \left(\frac{\tan\phi_{0-\mathrm{Plexiglas}} - s}{1 + \left(\frac{F_L}{F_D}\right)\tan\phi_{0-\mathrm{Plexiglas}}}\right) \left(\frac{\tan\phi_{0-\mathrm{alluvial}} - s}{1 + \left(\frac{F_L}{F_D}\right)\tan\phi_{0-\mathrm{alluvial}}}\right)^{-1} \tag{9.2}$$

where, for a given grain, $\phi_{0-\mathrm{Plexiglas}} = 26°$ is the friction angle found on a Plexiglas bed and $\phi_{0-\mathrm{alluvial}} = 60°$ is the friction angle found on an alluvial bed. Equation (9.2) assumes that all parameters are similar between the two cases (i.e., particle shape, size, flow hydraulics) except for the particle friction angle. Using $\frac{F_L}{F_D} = 0.8$ [*Wiberg and Smith*, 1985], $\tau_{c-\mathrm{alluvial}}^* = 0.03$, and S measured in our experiments or reported in the literature (Table 2), we find that planar beds can have τ_c^* as low as 0.007 (Table 2).

[19] The values of τ_c^* for nonalluvial and alluvial beds used in our analysis below are summarized and listed in Table 2. Note that the best data collapse for shear stress–based formulas (equation (6)) depends on good estimates of τ_c^*. We will show next that a fixed value of τ_c^* performs less well when predicting saltation trajectories across channels of varying roughness.

4. Results and Analysis

[20] Each subsection (sections 4.1–4.3) below is organized by first presenting the results from our flume experiments of saltating grains over smooth beds using a frequency distribution and standard deviation to illustrate the obtained data. Next, the mean value of each dependent variable (i.e., U_s, L_s, H_s) is given for comparison with published data. Sections 4.1, 4.2, and 4.3 treat downstream saltation velocity, saltation length, and saltation height, respectively. In section 4.4, we investigate the effect of particle angularity.

4.1. Grain Saltation Velocity

[21] We first tested the hypothesis that grain saltation velocity could vary with slope, especially when $S > 0.01$, even when local bed shear stress (τ_b) is approximately constant. Figure 3a shows the case where $\tau_b = 1.1$–1.5 N/m^2 (varied only slightly) and slope varied from 0.005 to 0.03 (Runs 1–4 in Table 1). Figure 3b shows the case where $\tau_b = 3.7$–4.2 N/m^2 and slope varied from 0.03 to 0.09 (Runs 5–8). With the exception of $S < 0.01$, results show that U_s increases monotonically with S (Figures 3a and 3b), but this is a relatively minor effect. Instead, the dominant effect is mean flow velocity (Figure 3d). Figure 3c shows that U_s also scales with bed stress, although U_s has a slightly stronger correlation with mean flow velocity (Figure 3d). Clearly the saltation velocity over a smooth bed can be characterized by either bed shear stress or flow velocity, as suggested by the dimensional analyses in section 2.

[22] Figure 4 shows that grain saltation velocity is independent of grain size. Using ANOVA test (analysis of variance), $F = 3.3$ and $p = 0.074$, which indicates that the mean values of the distributions of saltation velocities for all three grain sizes are statistically equal in Figure 4a (i.e., we cannot reject the null hypothesis that the means of the three

Table 2. Critical Shields Stress (τ^*_c) and Relative Bed Roughness (k_s/D) From Compiled Studies, Used in Figures 5a, 7a, and 9a

Data Source	Bed Type	R	τ^*_c	Method for τ^*_c	k_s (mm)	H/D	k_s/D
Nino et al. [1994]	Mobile alluvial	1.65	0.062–0.077	Formula in *Lamb et al.* [2008b]	23–60	2.6–4.8	1.5–2.0
Hu and Hui [1996]	Fixed alluvial	0.043–1.65	0.03	*Hu and Hui* [1996]	4.6–7.0	28–53	2.0
Hu and Hui [1996]	Smooth plane bed	0.043–1.65	0.007	Equation (9.2)	10^{-5}	23–54	$\sim 3 \times 10^{-6}$
Lee and Hsu [1994]	Fixed alluvial	1.64	0.026, 0.031	*Lee and Hsu* [1994]	1.4	19–89	1.0
Ancey et al. [2006, 2008]	Mobile alluvial	1.50	0.084	Formula in *Lamb et al.* [2008b]	15	0.8–6.8	2.5
Chatanantavet [2007]	Bedrock with grooves	1.65	0.015	*Chatanantavet* [2007]	2.4	3.3–20	0.10–0.34
Chatanantavet [2007]	Bedrock	1.65	0.03	*Chatanantavet* [2007]	2.7	4–18	0.11–0.40
This study	Smooth Plexiglas	1.65	0.007	Equation (9.2)	10^{-5}	1.5–24	4×10^{-7}–1.5×10^{-6}
Abbott and Francis [1977]	Plane bed	0.24–1.57	0.05	*Francis* [1973]	12.5	N/A	1.5
Francis [1973]	Fixed alluvial	1.42–2.2	0.05	*Francis* [1973]	10.2	6.9–7.3	1.5
Fernadez Luque and van Beek [1976]	Mobile alluvial	1.64	0.037–0.0455	*Fernandez Luque and van Beek* [1976]	2–6	N/A	2.0
Sekine and Kikkawa [1992]	Mobile alluvial	1.65	0.03	Assumed	7.5	N/A	1.5
Wiberg and Smith [1985]	Mobile alluvial	1.65	0.06	*Wiberg and Smith* [1985]	1–4	N/A	2

The physical bed roughness (k_s) has been quantified by using standard deviation of the bed [e.g., *Aberle and Smart*, 2003; *Finnegan et al.*, 2007; *Johnson and Whipple*, 2007] for "bedrock" beds such as *Chatanantavet* [2007]; using the method by *Kamphuis* [1974] for beds with fixed and mobile alluvial beds; and using the viscous sublayer for Plexiglas bed. "Bedrock" from the experiments of *Chatanantavet* [2007] refers to a roughened concrete bed (called "random abrasion 2" in his study).

distributions are the same at a 5% significance cutoff). One possible difference is for $D = 25$ mm, where the frequency distribution is skewed to lower values of U_s. We attribute this to the fact that the 25 mm grains alone were almost perfectly spherical. Since the centroid position of particle mass of spherical grains helps transfer momentum onto the bed [e.g., *Schmeeckle et al.*, 2001], the 25 mm grains bounced relatively higher than grains of $D = 6.7$ and 13.4 mm and even occasionally jumped above the water surface during saltation. This effect particularly stands out when the water depth was shallow (lower H/D ratio) and Fr number was high; for example, in the case of $S = 0.09$ in Figure 4b where for $D = 25$ mm, 47 % of saltating grains jumped out of the water, notably reducing U_s relative to smaller grain sizes. As this appears to be uncommon in natural settings (H/D is exceptionally low in run 9 for $D = 25$ mm and natural grains are rarely almost perfectly spherical), we conclude that saltation velocity is independent of grain size (Figure 4b) for saltating bed load regime.

[23] In Figure 5, we combine new and published data on mean grain saltation velocity over various types of bed surface ranging from smooth Plexiglas bed from our experiments reported here, to moderate bedrock roughness [*Chatanantavet*, 2007], to a fully mobile alluvial bed [*Nino et al.*, 1994; *Ancey et al.*, 2006, 2008]. Figure 5a illustrates how using equation (6.1) with grain size as the normalizing length scale (i.e., $U_s/(RgD)^{0.5}$) fit the data well for all bed roughness types, provided a correct assessment of critical Shields stress that incorporates bed roughness and slope is used in all cases (see Table 2 for the critical Shields stress for each data set used in Figure 5a). For published data on steep slopes, we accounted for a heightened τ^*_c with S using the theory of *Lamb et al.* [2008b], which in general improved the data collapse (e.g., for the case of *Nino et al.* [1994]). Figure 5b illustrates the same data set and empirical formula as in Figure 5a, except that $\tau^*_c = 0.03$ has been used for all data (i.e., instead of values in Table 2), which is a common assumption. This results in more data scatter and underestimation of U_s for smooth beds and overestimation of U_s for alluvial beds. Since saltation parameters have been shown to influence erosion rate of bedrock channels [e.g., *Sklar and Dietrich*, 2004; *Lamb et al.*, 2008a], landscape evolution models that possess τ^*_c [e.g., *Tucker and Slingerland*, 1997; *Whipple and Tucker*, 2002; *Gasparini et al.*, 2006, 2007; *Crosby et al.*, 2007; *Sklar and Dietrich*, 2006] may need to consider this issue carefully regarding model assumptions.

[24] Following results in Figure 3d, where $U_s = 0.8U$, we find that using water depth as a length scale and plotting nondimensional U_s against nondimensional flow velocity U (leading to Fr as an independent variable) collapses the experimental data of U_s better than in Figure 5a for all types of bed roughness (Figure 5c). We fit a power law to the data in Figure 5c using a stepwise regression and found

$$\frac{U_s}{\sqrt{gH}} = 0.6\,Fr \tag{10.1}$$

or

$$U_s/U = 0.6 \tag{10.2}$$

where the exponent of 1.0 ± 0.04 (mean $\pm$ uncertainty) and the coefficient of 0.6 ± 0.05 achieved the best least squares fit ($r^2 = 0.9$) The data set has wide ranges of values

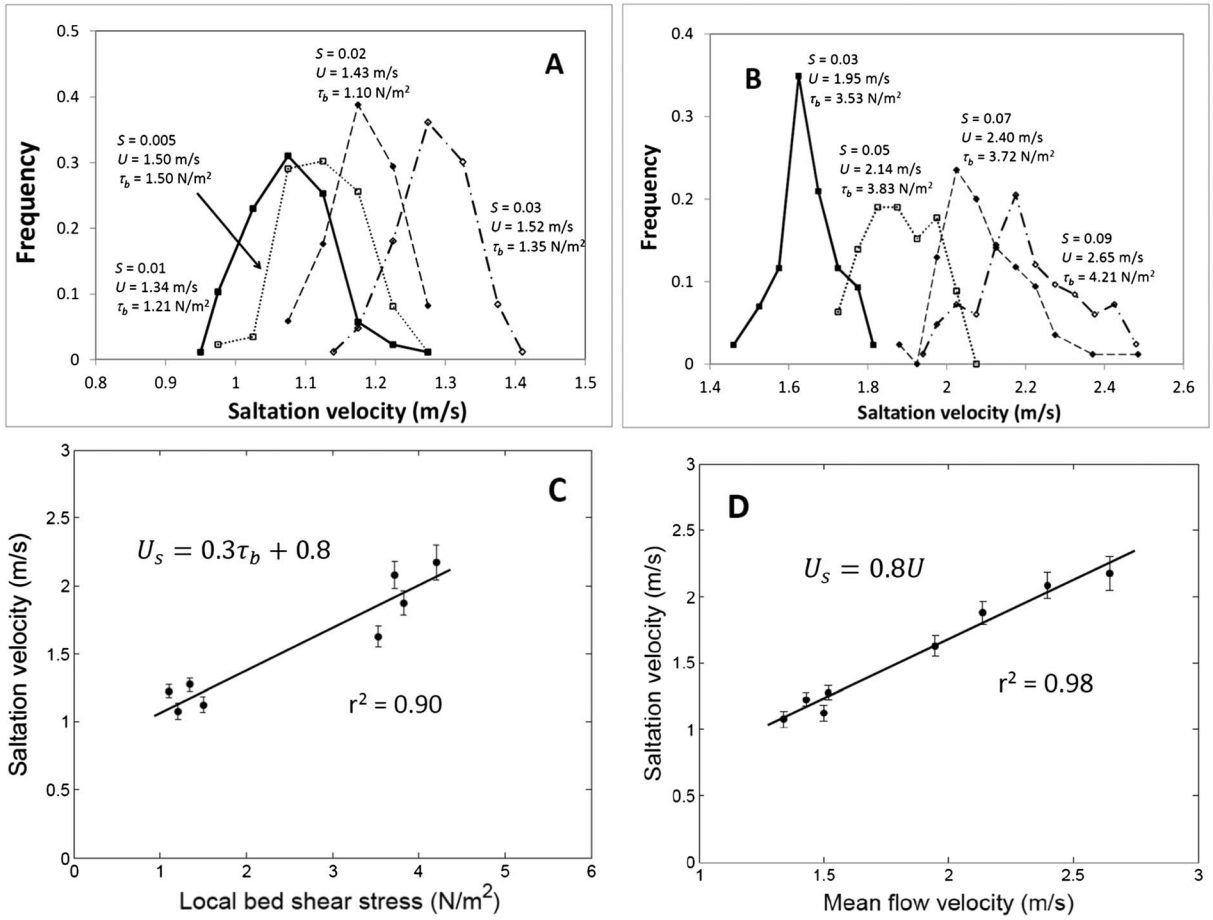

Figure 3. Frequency distributions of grain saltation velocity under various slopes while fixing bed shear stress nearly constant. (a) $\tau_b = 1.1$–$1.5\ \mathrm{N/m^2}$ (runs 1–4) and (b) $\tau_b = 3.5$–$4.2\ \mathrm{N/m^2}$ (runs 5–8). The grains used here have $D = 6.7$ mm. (c) Plot of U_s versus bed shear stress using data in Figures 3a and 3b. Error bars represent the standard deviation. (d) Plot of U_s versus mean flow velocity.

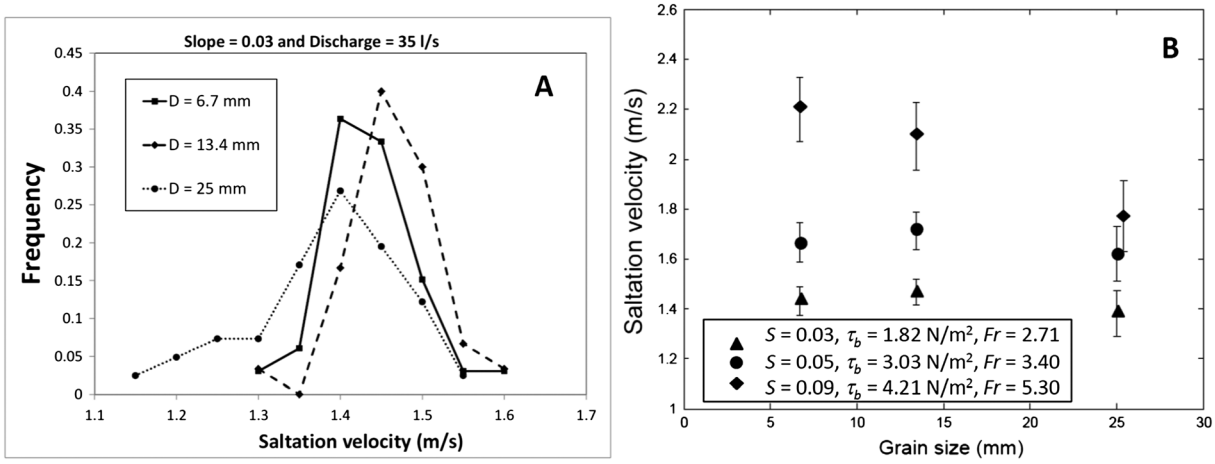

Figure 4. (a) Comparison of frequency distribution of grain saltation velocity for three different grain sizes (ANOVA: $F = 3.3$, $p = 0.074$). Hydraulic conditions correspond to run 9 in Table 1, on planar Plexiglas bed. (b) Comparison of saltation velocity for different slopes, bed shear stresses, Froude numbers, and grain sizes corresponding to runs 8–10 (Table 1), on planar Plexiglas bed. Mean values with one standard deviation are shown.

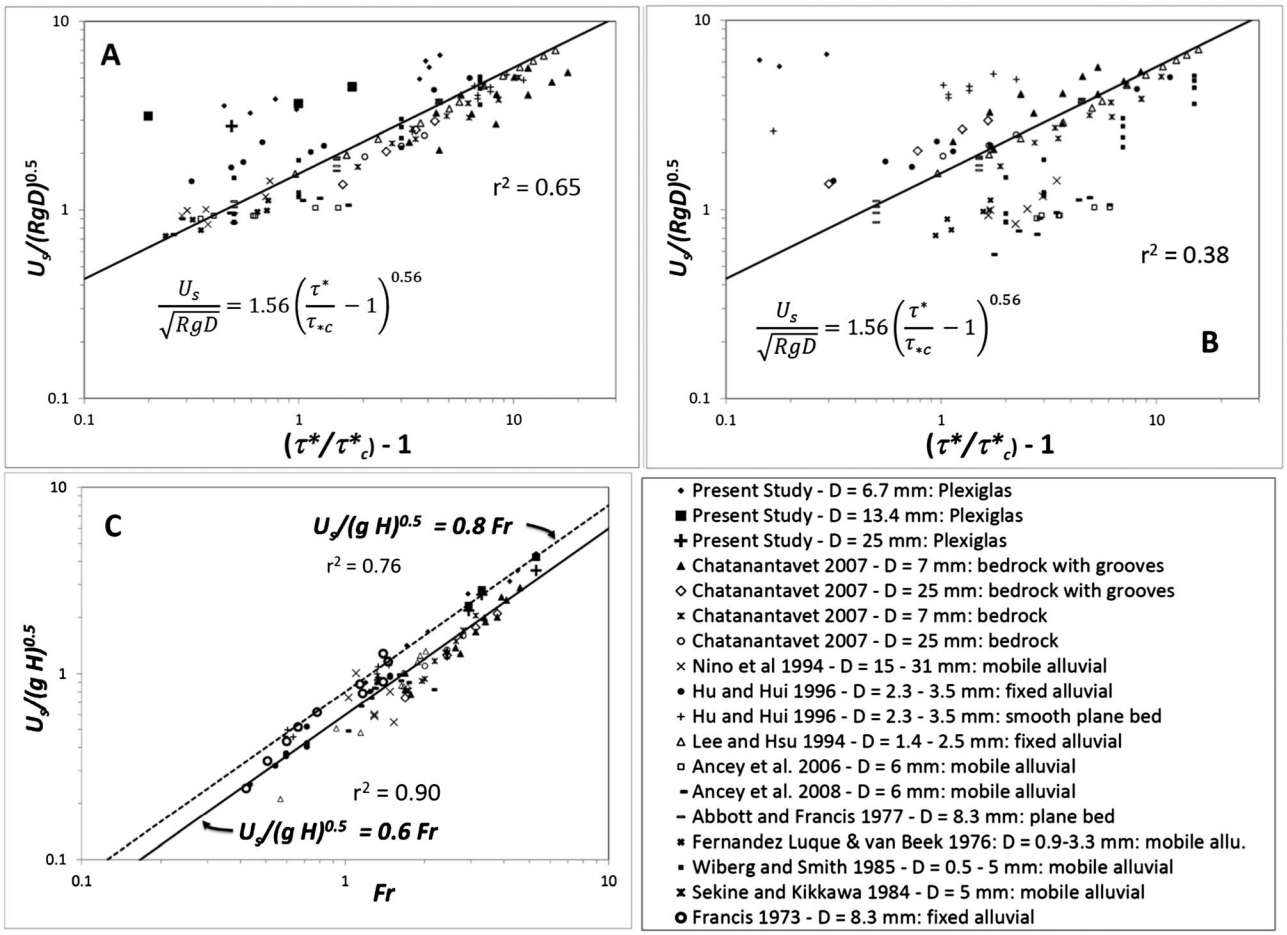

Figure 5. (a) Shear stress–based, empirical formula for mean saltation velocity by *Sklar and Dietrich* [2004] and experimental data using τ^*_c values in Table 2. (b) Same data set and formula in Figure 5a, except that constant $\tau^*_c = 0.03$ has been used for all data (i.e., instead of values in Table 2). Note that many data for the Plexiglas bed would have negative values of $(\tau^*/\tau^*_c) - 1$ and consequently are not plotted here. (c) Froude number–based, empirical formula for grain saltation velocity. The values of H/D ratio in this plot vary from 1 to 90. Not all data in Figure 5a can be plotted in Figure 5c because some data sets only report shear stress and not velocity, and vice versa. All runs in Table 1 have been used here.

of H/D (0.8–89), R (0.043–2.2), and k_s/D (4×10^{-7}–2.5) (Table 2), yet these three parameters appear not to affect saltation velocity.

[25] From equation (10.2), it can be seen that grain saltation velocity is about 60% of depth-averaged flow velocity. Note this is slightly different than 80% found from our experiments (Figure 3d) due to the inclusion of other data sets; however, both equations fit the data quite well ($r^2 = 0.9$ for a coefficient of 0.6 and $r^2 = 0.76$ for a coefficient of 0.8; Figure 5c). As seen in Figure 5c that data from smoother beds are plotted more or less on top of alluvial beds, this discrepancy of ratio coefficients between Figure 3d and Figure 5c should not be interpreted as due to different bed conditions. In other words, there is no systematic difference regarding this plot of U_s versus U between smooth and rough beds. Note that plotting all data in dimensional form (U_s versus U), similar to Figure 3d, yields as strong a correlation as shown in Figure 5c; hence, the strong correlation is not an artifact of $\sqrt{gH}$ appearing in both the dependent and independent variables (the same argument applies to scaling L_s and H_s below). Note also that k_s/D varies significantly from ≈ 1–3 for mobile alluvial bed data with uniform grains to much smaller values in our flume with smooth Plexiglas bed (in which k_s depends on the thickness of the viscous sublayer) or in Chatanantavet's data for bedrock beds, as shown in Table 2. In addition, the data of *Hu and Hui* [1996] show submerged specific density values (R) ranging from 0.043 to 1.65 (total of 19 data points), yet the data are fitted by equation (10) well. This suggests that generally mean saltation velocity of grains is not only independent of grain size but also independent of R. However, in the case of saltation hop length, it is found that R is important for scaling as shown in the next section.

4.2. Grain Saltation Length

[26] Figure 6a shows frequency distributions of saltation hop lengths for different values of slope, Froude number, and bed shear stress for grain size of $D = 6.7$ mm on a smooth Plexiglas bed. The bed shear stress ranges from 1.2 to 4.2 N/m^2 and Froude number ranges from 1.32 to 5.30.

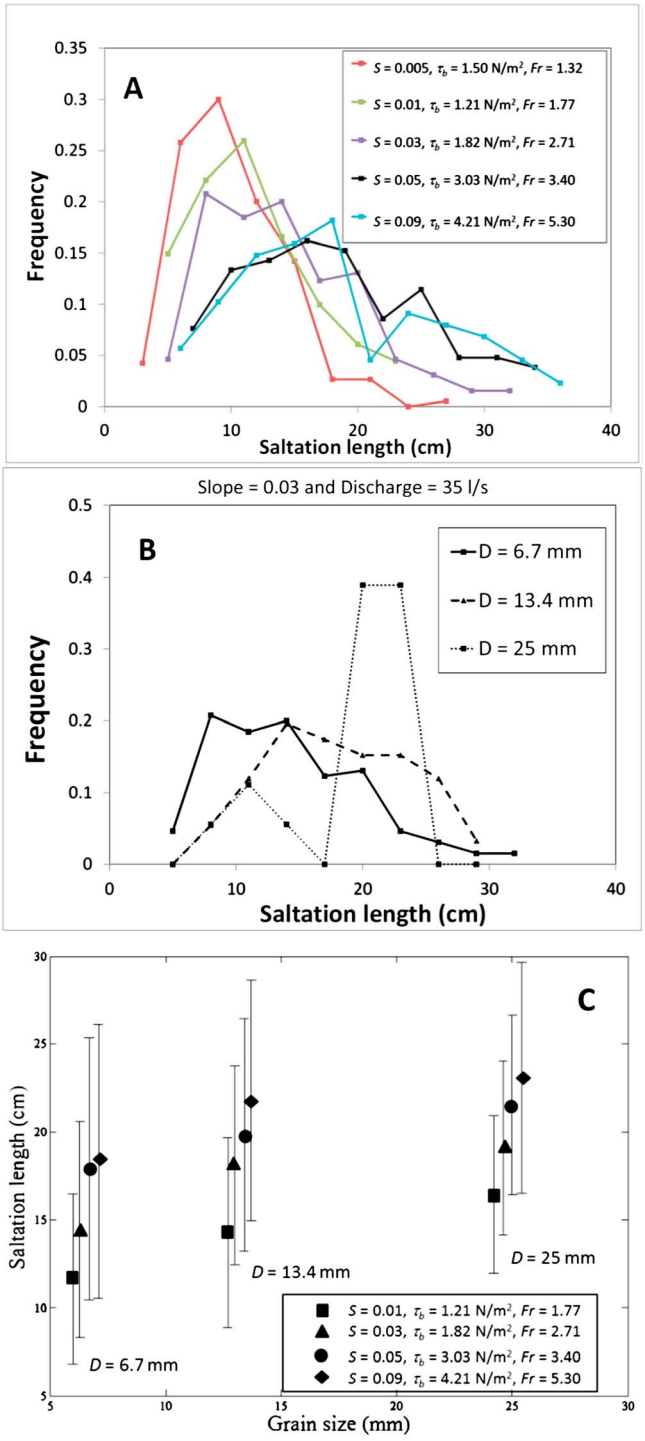

Figure 6. (a) Frequency distribution of saltation hop lengths for different values of bed slope, Froude number, and bed shear stress using $D = 6.7$ mm only. Hydraulic conditions correspond to runs 1, 2, 9, 10, and 8 in Table 1. (b) Frequency distribution of saltation lengths for three different bed load grain sizes for run 9 (ANOVA: $F = 26$, $p < 0.0001$). (c) Comparison of saltation hop length for different slopes, bed shear stresses, Froude number, and grain sizes for runs 2, 9, 10, and 8. Mean values with one standard deviation are shown.

The saltation lengths for each hydraulic condition vary considerably. For example, for $\tau_b = 1.50$ N/m^2, L_s can range from 2 to 22 cm (Figure 6a). For $\tau_b = 4.21$ N/m^2, L_s ranges from 5 to 36 cm, and the frequency distribution is skewed. Mean L_s increases with increasing shear stress or Froude number (Figure 6c). In addition, saltation length increases slightly with increasing grain size (Figures 6b and 6c). In Figure 6b, for example, using ANOVA, $F = 13$ and $p < 0.0001$, which indicates that the mean values of saltation length distributions for these three different grain sizes are statistically different (i.e., we can reject the null hypothesis that the means of the distributions are the same at a 0.01% significance cutoff).

[27] Figure 7a illustrates that a shear stress–based formula for estimating L_s (equation (6.2)) fits the data reasonably well for both smooth beds and alluvial beds using different τ_c^* for different data sets (Table 2). In keeping with our *Fr*-based analysis of saltation velocity, here we explored whether nondimensional saltation length (L_s/H) varied systematically with Froude number, submerged specific density R, and nondimensional grain size (D/H). As shown in Figure 7b, we find a power law relationship that matches the data for all bed roughness types ranging from smooth to mobile alluvial bed and R from 0.043 to 1.65, as

$$\frac{L_s}{H} = 2\left(Fr\left(\frac{D}{H}\right)^{0.25} R^{-0.5}\right) \tag{11.1}$$

or its dimensional form,

$$L_s = \frac{2}{\sqrt{gR}} U(HD)^{0.25}. \tag{11.2}$$

[28] We determined these exponents using stepwise multiple regression by systematically conducting trial-and-error on the exponents of *Fr* and *D/H* first and arrived at 1 ± 0.03 (mean $\pm$ uncertainty) and 0.25 ± 0.01, respectively, to achieve the highest value of r^2. Since the variation of R values only exists for one data set [*Hu and Hui*, 1996] (19 data points), we conducted this regression last and found a collapse of the data with the exponent of -0.5 ± 0.03 and a coefficient of 2 ± 0.05. The saltation hop length is positively but weakly proportional to water depth and grain size raised to the power of 0.25, but linearly proportional to flow velocity. Lighter particles (lower R) also have longer hop lengths than heavier particles. The *Fr*-based scaling yields a better fit than the bed stress–based scaling (Figure 7). In Figure 7b, the relative roughness k_s/D varies significantly from ≈ 1 to 3 for alluvial bed data with uniform grains to a much smaller value in our flume with Plexiglas bed, supporting the unimportance of k_s/D in the *Fr*-based scaling.

4.3. Grain Saltation Height

[29] Figure 8a shows frequency distributions of saltation hop heights for different slopes, Froude numbers, and bed shear stresses for a grain size of $D = 6.7$ mm on a smooth Plexiglas bed. The bed shear stress ranges from 1.2 to 4.2 N/m^2, and Froude number ranges from 1.32 to 5.30. The experimental data for all hydraulic conditions collapse

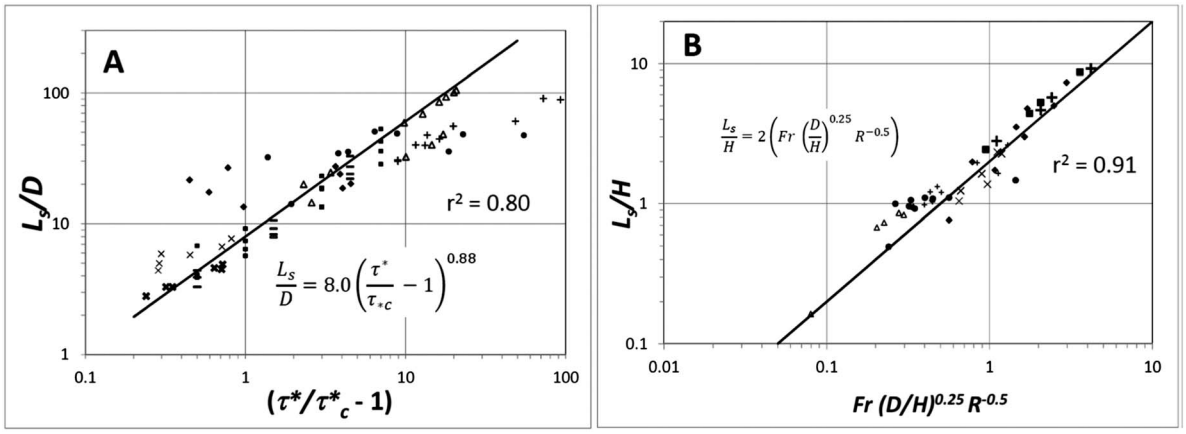

Figure 7. (a) The bed shear stress–based scaling for saltation length fit by a relation from *Sklar and Dietrich* [2004] with bed roughness varying from smooth planar bed to mobile alluvial bed. τ_c^* from Table 2 is used. (b) The Froude number–based scaling for saltation length with bed roughness from smooth bed to mobile alluvial bed and R varying from 0.043 to 1.65. Runs 2, 8, 9, and 10 in Table 1 have been used here. See the symbol legend in Figure 5. Only data with known velocity values are included in Figure 7b.

to the same relationship. The values of H_s range from 2 to 27 mm, with a mean value of about 8 mm. It appears, however, that saltation height is sensitive to grain size (Figures 8b and 8c). In Figure 8b, for example, using ANOVA, the mean values of saltation height distributions for these three different grain sizes are statistically different ($F = 34$ and $p < 0.0001$). The frequency distribution becomes wider as grain size increases (Figures 8b and 8c). Mean saltation height, H_s, appears to be insensitive to bed shear stress and Froude number (Figure 8c).

[30] Figure 9a illustrates that a shear stress–based formula for estimating H_s (equation (6.3)) fits the data well for both smooth beds and alluvial beds; variable τ_c^* values are used here (Table 2). Similar to our treatment of saltation lengths, we explore whether nondimensional saltation height (H_s/H) varied systematically with Froude number and nondimensional grain size (D/H) as well as R. As shown in Figure 9b, we find a scaling relationship for all types of bed roughness ranging from smooth to mobile alluvial bed as

$$\frac{H_s}{H} = 0.6\left(Fr\left(\frac{D}{H}\right)^2\right)^{0.3} \tag{12.1}$$

or in its dimensional form

$$H_s = \frac{0.6}{g^{0.15}} H^{0.25} U^{0.3} D^{0.6}. \tag{12.2}$$

[31] Again, we determined these exponents for Fr, R, and D/H using stepwise multiple regression by systematically conducting trial-and-error on the exponents of Fr and D/H first and arrived at the exponents 0.3 ± 0.02 (mean ± uncertainty) and 0.6 ± 0.03, respectively, to achieve the highest value of r^2. We found no significance of R in the scaling although 19 data points from *Hu and Hui* [1996] have various values of R from 0.043 to 1.65. Therefore, submerged specific density (R) is not included here. The coefficient was then determined as 0.6 ± 0.02. As in the saltation length analysis, we found no significance of the relative bed roughness k_s/D in the Fr-based scaling.

[32] By including data from the literature, we resolve a hydraulic dependency for mean H_s that was not apparent in Figure 8, in that saltation height is weakly dependent on water depth and flow velocity. This makes sense since lift and drag forces scale with both U and D, and it is the resultant force that acts on the particle and produces a specific trajectory [e.g., *Wiberg and Smith*, 1985]. The Fr-based scaling yields a better fit than the bed stress–based scaling (Figure 9) due to uncertainty in τ_c^*.

4.4. Effect of Grain Shape

[33] One may ask "how transferable is this study to angular grains?" In steep bedrock channels, fresh angular materials perhaps dominates the sediment supply although subrounded particles are ubiquitous farther downstream of bedrock rivers. To test for the effect of grain angularity, we conducted experiments comparing the saltation characteristics between subrounded grains and angular grains, both with $D = 6.7$ mm (Figure 10a) and for the hydraulic conditions of run 10 (Table 1). Over the smooth Plexiglas bed, only 6% of subrounded grains were sliding or rolling on the bed during transport while the rest were in saltation. In contrast, results from the angular grains showed that 37% of grains were in a sliding mode, and the rest were in saltation. This large fraction of sliding grains is likely due to the very smooth Plexiglas bed. Natural streambeds are never perfectly smooth and perturbations on even the smoothest natural bedrock beds may cause most grains to saltate.

[34] Saltation data from both angular and subrounded grains are comparable (Figures 10b–10d), excluding the sliding or rolling grains. There seems to be no considerable difference of saltation velocity between subrounded and angular grains (Figure 10b); the mean values ($\pm 1\sigma$) are 1.71 ± 0.08 and 1.67 ± 0.08 m/s, respectively, which are within the margin of variability. Using ANOVA, the mean

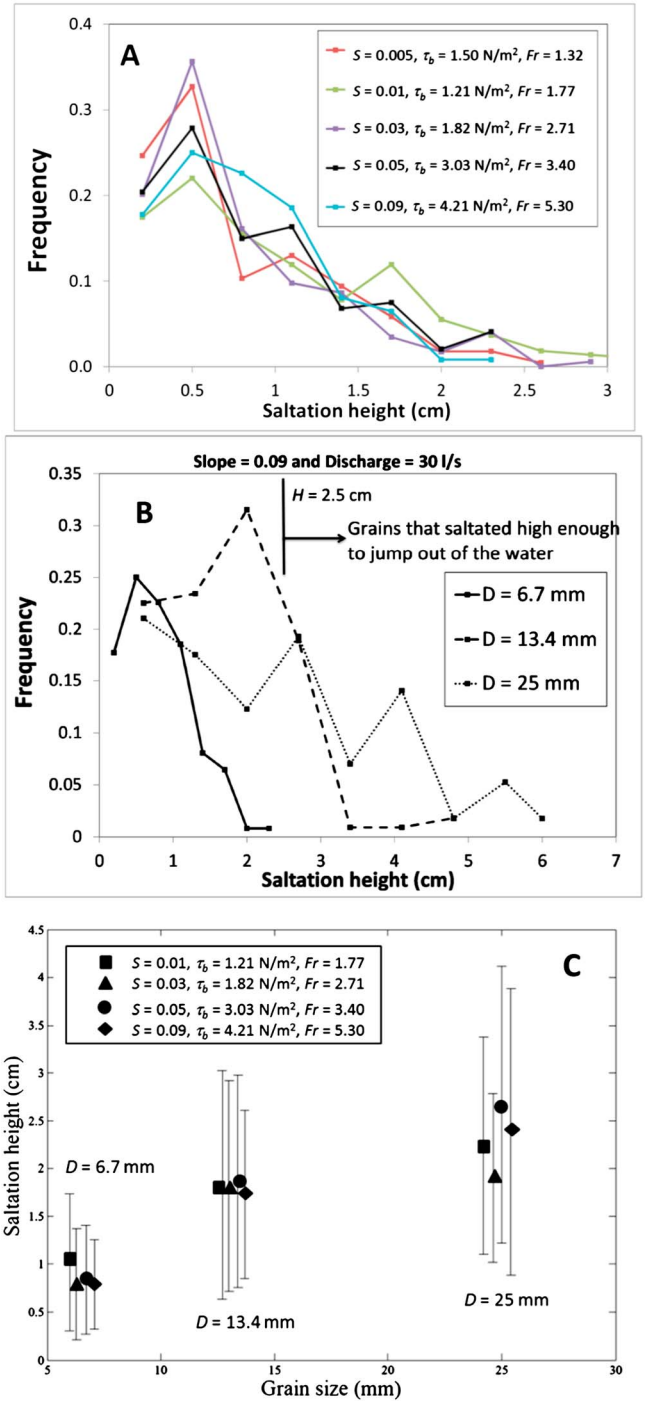

Figure 8. (a) Frequency distribution comparison of saltation hop heights for different values of bed slope, Froude number, and bed shear stress using $D = 6.7$ mm for runs 1, 2, 9, 10, and 8 (Table 1). (b) Frequency distribution comparison of saltation height for three different bed load grain sizes (ANOVA: $F = 34$, $p < 0.0001$). Note that, unlike plots of L_s in Figures 6b and 6c, the range of H_s (and thus the standard deviation) increases with grain size. About half of the bed load with $D = 25$ mm saltated high enough to jump out of the water (run 8; i.e., for $H_s > H = 2.5$ cm. (c) Comparison of saltation height for different slopes, Froude number, bed shear stresses, and grain sizes for runs 2, 9, 10, and 8. Mean values with one standard deviation are shown.

values of the saltation velocity distributions for these two grain shapes are however statistically different ($F = 10$ and $p = 0.002$), though slightly. The saltation height and length for subrounded grains are slightly larger than ones for angular grains (Figures 10c and 10d), although they are well within the 1 standard deviation. For subrounded grains, the mean values ($\pm 1\sigma$) of H_s and L_s are 0.84 ± 0.57 and 17.9 ± 7.4 cm, respectively. In contrast, for angular grains, the mean values ($\pm 1\sigma$) of H_s and L_s are 0.56 ± 0.38 and 16.0 ± 7.3 cm, respectively. Using ANOVA, the mean values of saltation length distributions for these two grain shapes are statistically the same ($F = 2.4$, $p = 0.13$). For saltation height, the mean values of the distributions for these two grain shapes are statistically different ($F = 9.6$, $p = 0.0025$). The overall results indicate that subrounded grains have slightly more pronounced hops over smooth plane beds than angular grains, but within the observed variability, the saltation dynamics between the two grain shapes are similar.

5. Discussion

[35] The present study pertains to saltation dynamics of coarse bed load on both nonalluvial, nonerodible beds and mobile alluvial beds. Our results indicate that both shear stress–based and *Fr*-based scalings are valid for characterizing bed load saltation dynamics (saltation velocity, hop height, and hop length) as a function of flow hydraulics over a range of bed roughnesses ranging from smooth planar beds to alluvial beds. However, the *Fr*-based formulas have advantages that (1) there is no need to estimate a critical Shields stress $\left(\tau_c^* = f\left(S, \frac{k_s}{D}, R\right)\right)$, which could vary up to 2 orders of magnitude (e.g., 0.001–0.1 from *Hodge et al.* [2011]) from very smooth bedrock beds to alluvial beds, to very rough bedrock beds, and (2) the *Fr*-based scaling fits the saltation data set better than the shear stress–based scaling (Figures 5, 7, and 9). The *Fr*-based scaling promises to be particularly useful in analysis of laboratory studies of abrasion of rock beds with little or no alluvial cover. Conversely, it may be easier to estimate reach-averaged bed shear stress than to estimate flow velocity (and *Fr*) in natural bedrock rivers unless there is a gauge installed. In the field researchers will face either the challenge of estimating flow velocity (e.g., using the most suitable roughness coefficient) [e.g., *Ferguson*, 2010; *Rickenmann and Recking*, 2011] and *Fr* or the challenge of characterizing critical Shields stress values as a function of bed state, channel slope, and flow conditions [e.g., *Lamb et al.*, 2008b].

[36] Our results in Figure 5b also show that assuming $\tau_c^* = 0.03$ (or any other fixed value of τ_c^*) does not sufficiently characterize the bed load saltation dynamics, and any landscape evolution models that use a constant value of τ_c^* [e.g., *Tucker and Slingerland*, 1997; *Whipple and Tucker*, 2002; *Gasparini et al.*, 2006, 2007; *Crosby et al.*, 2007; *Sklar and Dietrich*, 2006] should take this into account. Both slope and relative bed roughness (k_s/D) vary considerably in mountainous bedrock rivers, including mixed bedrock-alluvial conditions. For example, rock bed roughness alone can vary significantly from smooth bedrock (Figure 11a) to very rough rock bed forms (Figure 11c).

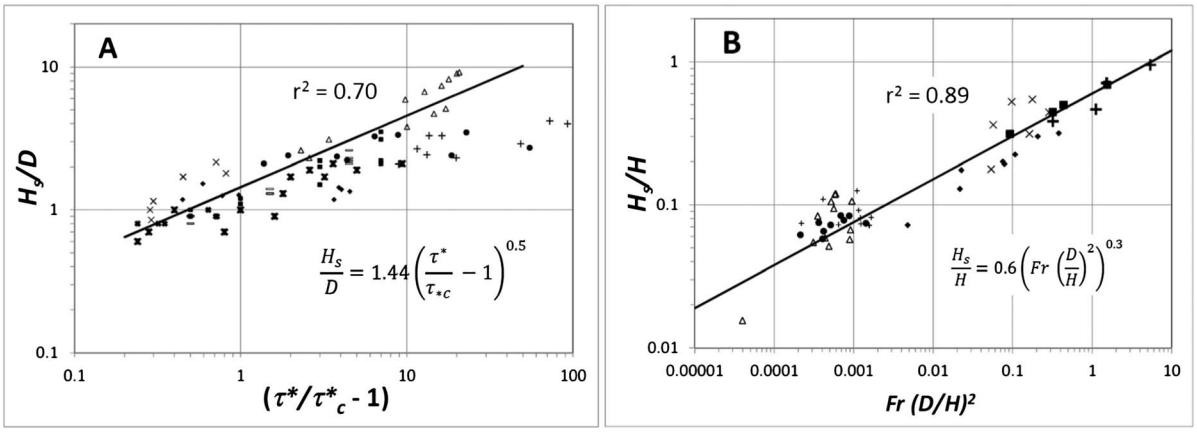

Figure 9. (a) The bed shear stress–based scaling for saltation height compared to a relation from *Sklar and Dietrich* [2004] with bed roughness varying from smooth planar beds to mobile alluvial beds. (b) The Froude number–based scaling for saltation height with bed roughness from smooth bed to mobile alluvial bed. Runs 2, 8, 9, and 10 in Table 1 have been used here. See the symbol legend in Figure 5. Only data with known velocity values are included in Figure 9b.

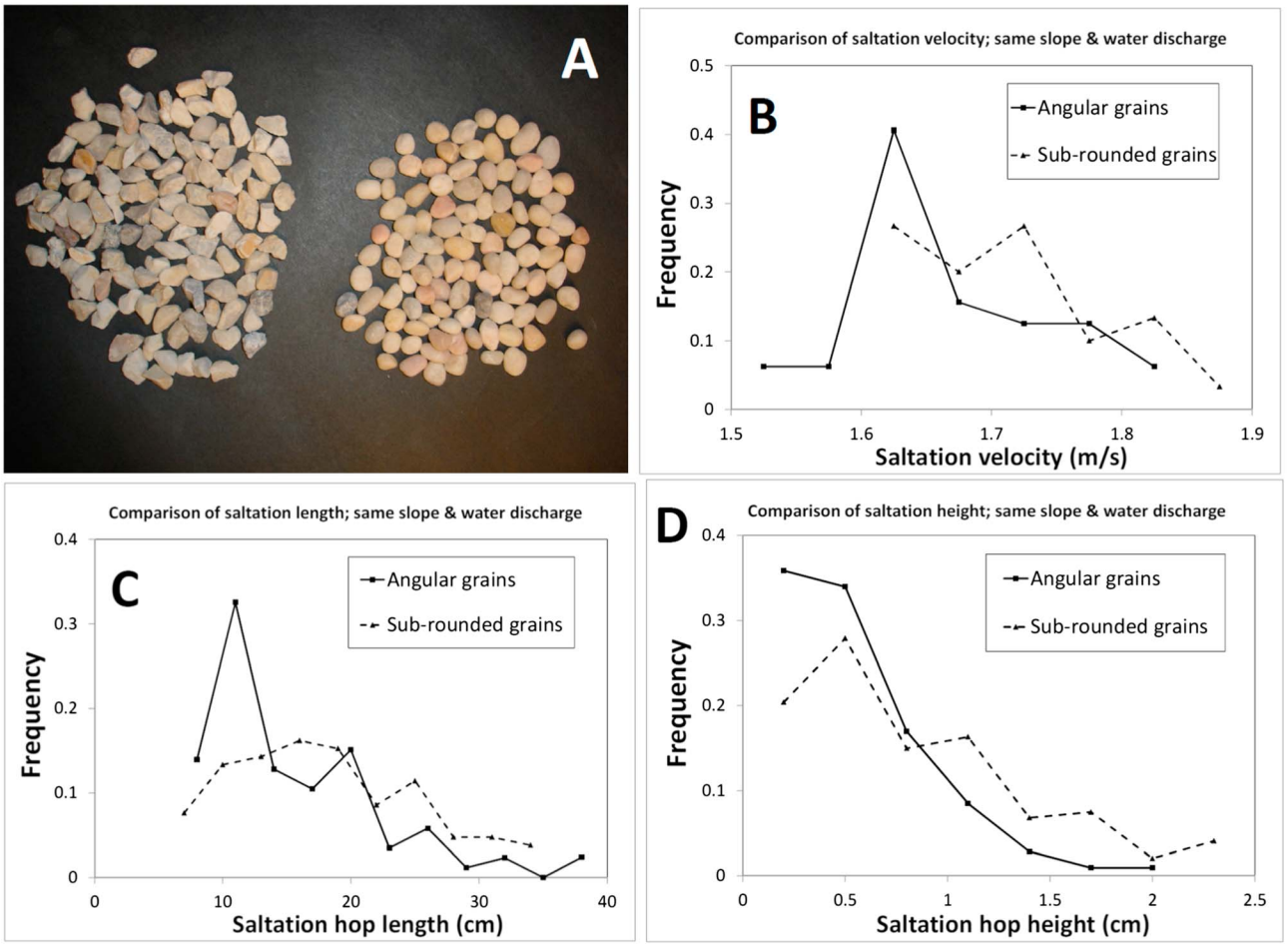

Figure 10. (a) Pea gravels ($D = 6.7$ mm) used in the comparison of saltation dynamics between angular (left) and subrounded (right) grains. (b) Comparison of saltation velocity frequency distribution between the angular and subrounded grains (ANOVA: $F = 10$, $p = 0.002$). (c) Comparison of saltation length frequency distribution (ANOVA: $F = 2.4$, $p = 0.13$), and (d) comparison of saltation height frequency distribution (ANOVA: $F = 9.6$, $p = 0.0025$). The hydraulic conditions are for run 10 in Table 1 and are the same for all cases.

Figure 11. Different bedrock rivers with different bed roughness. (a) A bedrock stream in Japan (Image Source: Gary Parker); (b) an unnamed, steep bedrock channel in Northern California, USA (the valley top width is about 20 m); and (c) the Val Verzasca River Valley, Italy. The channel width is about 50 m.

[37] Our new *Fr*-based scaling indicates that the saltation velocity of bed load appears to be independent of grain density and grain size. Interestingly, *Hodge et al*. [2011] also found size-independent travel distances of bed load tracers in a predominantly bedrock-bedded river. Grain saltation velocity appears to be a linear function of flow velocity. Saltation height is primarily sensitive to grain size. This is reasonable as higher drag and lift forces acting on the grain are associated with larger particle diameters. Saltation length increases primarily with flow velocity and the inverse of the square root of submerged specific density, which is sensible considering that with the same force acting on a particle of size D, a lighter particle would be transported farther in a single hop. The saltation height, on the other hand, is not sensitive to particle density.

[38] Although it is difficult to estimate *Fr* during extreme floods, field observations of bedrock rivers during floods have often found supercritical flow conditions ($Fr > 1$) [e.g., *Tinkler and Parish*, 1998; *Turowski and Rickenmann*, 2009]. We suspect that for bedrock rivers with relatively smooth beds and steep slopes (e.g., Figures 11a and 11b), Froude numbers can be highly supercritical, particularly in those reaches where the rock bed is frequently exposed. Importantly, we find the same scaling of saltation parameters with Froude number in both subcritical and supercritical flows (Figures 5, 7, and 9).

[39] Many bedrock rivers have very rough beds (e.g., Figure 11c), which may affect the applicability of our empirical formulas that are based on alluvial beds, smooth planar beds, and rock beds with minor roughness where relative bed roughness $k_s/D \leq 3$. The flow velocity profile over very rough beds ($k_s/D >> 3$) or inside a narrow slot canyon could be different than in our experiments, which could affect saltation dynamics. Furthermore, protruding rocks with extreme topography (e.g., Figure 11c) may act as immobile boulders and form drag concepts such as those of *Yager et al*. [2007] and studies such as those by *Nitsche et al*. [2011], *Egashira and Ashida* [1991], and *Pagliara and Chiavaccini* [2006] may need to be employed. In addition, *Goode and Wohl* [2010] found that the extent to which grain travel distances are dependent on grain size is a function of bedrock bed structure.

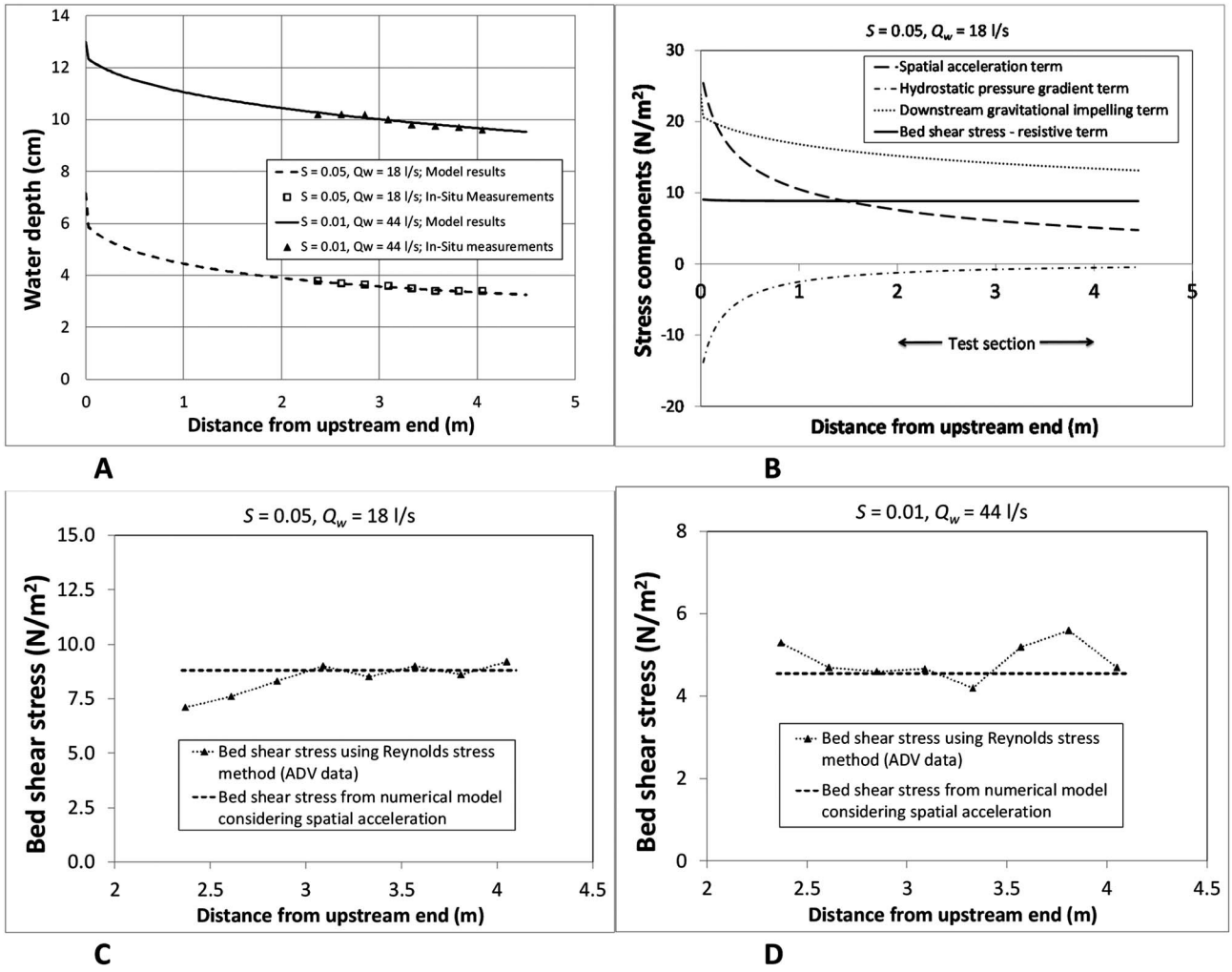

Figure A1. (a) Calibration of measured water depth and the flow model (equation (A3)). (b) Model results of multiple stress components from equation (A4). Note that our test section, in which the hydraulic conditions (Table 1) and saltation parameters were measured, is in $x = 2$–4 m where the flow acceleration effect is much less than the upstream area. (c and d) Comparison of the bed shear stress values between the measured Reynolds stresses and from the model (equation (A4)) for two different hydraulic conditions.

6. Conclusion

[40] The present study consists of a detailed experimental investigation of saltation dynamics of coarse grains on a smooth, hard surface. Using both our data and data from the literature, we developed two sets of empirical formulas for particle saltation velocity, hop height, and hop length under variation of bed roughness, bed shear stress, Froude number, and particle size. We found that both shear stress–based and *Fr*-based scalings are valid in characterizing bed load saltation dynamics over different bed roughnesses. However, *Fr*-based scaling yields a better fit to all saltation data (saltation velocity, hop height, and hop length), and it has an advantage over the traditional bed shear stress–based scaling in that there is no need to estimate a critical Shields stress τ_c^*, which is hard to do considering wide ranges of bed roughness and slope in bedrock rivers. Results show that the saltation velocity of bed load is independent of grain density and grain size and scales linearly with flow velocity. Saltation height has a nonlinear dependence on grain size, and saltation length increases primarily with flow velocity and it is inversely proportional to submerged specific density. In natural streams, researchers will face either the challenge of estimating flow velocity (via roughness coefficient) and *Fr* or the challenge of characterizing τ_c^*. Since saltation parameters have been shown to influence erosion rate of bedrock channels [e.g., *Sklar and Dietrich*, 2004; *Lamb et al*., 2008a], landscape evolution models that employ τ_c^* [e.g., *Tucker and Slingerland*, 1997; *Whipple and Tucker*, 2002; *Gasparini et al*., 2006, 2007; *Crosby et al*., 2007; *Sklar and Dietrich*, 2006] may need to consider this issue carefully.

Appendix A: Procedure for quantification of bed shear stress in our flume

[41] Conducting flume experiments in a steep channel where the flow is supercritical ($Fr > 1$) creates spatial acceleration (nonuniform flow), where the water flows from

an upstream headbox through honeycomb to the channel. This is because the flow depth changes from the critical depth (H_c) at the headbox upstream (where $Fr = 1$) to normal depth downstream (where $H_n < H_c$). This generates an S2 water surface curve [e.g., *Chow*, 1959]. Our flume channel did not have an adequate length for the water depth to completely transform to a uniform value in our test section where the saltation parameters and hydraulic variables were measured. However, we can accurately calculate the bed shear stress in our test section accounting for flow acceleration.

[42] Conservation of fluid mass and momentum of depth-averaged, 1-D flow in the streamwise (x) direction for a channel for a channel with uniform wall and bed roughness can be written as [e.g., *Chow*, 1959]

$$\frac{d(UH)}{dx} = 0 \tag{A1}$$

$$U\frac{dU}{dx} = -g\frac{dH}{dx} + gS - C_f\frac{U^2}{R_b} \tag{A2}$$

where C_f is a friction coefficient and R_b is the hydraulic radius. The combination of equations (A1) and (A2) leads to a formulation of the backwater equation [*Chow*, 1959] for narrow channels as

$$\frac{dH}{dx} = \frac{s - C_f\frac{U^2}{gR_b}}{1 - Fr^2}. \tag{A3}$$

[43] The equation (A2) can be rearranged to

$$\tau_b = \rho g R_b S - \rho g R_b\frac{dH}{dx} - \rho U R_b\frac{dU}{dx} \tag{A4}$$

where the left-hand side parameter is bed shear stress or resistive term ($\tau_b = \rho C_f U^2$), the first term on the right-hand side (RHS) represents the downstream gravitational impelling stress, the second term on the RHS represents the hydrostatic pressure gradient, and the last term on the RHS represents the spatial acceleration.

[44] The calculation procedure to obtain each component in equation (A4) proceeds as follows: First, the slope, water discharge, channel width, and Manning's n coefficient (e.g., 0.01 for smooth glass or concrete bed) are specified. From known water discharge (Q_w), a critical depth (H_c) can be calculated—this would be the water depth for the node at upstream end. After knowing R_b at the upstream end node, we can estimate friction coefficient there as well from $C_f = \frac{gn^2}{R_b^{1/3}}$. In order to avoid a discontinuity at $Fr = 1$ (where the RHS term in equation (A3) goes to infinity), slightly higher value of Fr (e.g., 1.03) for the critical flow condition is specified at the upstream node. Then we solve the differential equation (A3) to obtain $H(x)$ one step downstream using the prediction-correction scheme. The value of $C_f(x)$ can be revised as H is solved. The values of $U(x)$ and $\tau_b(x)$ would thus be obtained. Since we have the in situ measured water depth values from the flume, we are able to verify our results of $H(x)$ against the measured data (Figure A1-a). In order to get the best match, it may be necessary to slightly adjust Manning's n value accordingly; for smooth bed (Plexiglas or planar concrete bed) Manning's n should range between 0.009 and 0.013 [e.g., *Chow*, 1959]. Finally, we obtain the calibrated values of $H(x)$, $U(x)$, and $\tau_b(x)$. We can also calculate each term in equation (A4) and compare their relative importance (Figure A1-b).

[45] The calculated bed shear stress values have been verified with measured values of the near-bed Reynolds stress using velocity data taken using an acoustic Doppler velocimeter (ADV) for select runs (Figure A1). Figures A1-c and A1-d illustrate the comparisons of bed shear stress values from the Reynolds stress (ADV) and the calibrated model (equation (A4)). Note that bed stress is not calculated from the log-law profile since this assumed uniform flow. Note also that our calculations (not shown here) show that mean flow velocity increases with increasing slope while holding τ_b constant for this case of spatial flow acceleration.

[46] **Acknowledgment.** This work was supported by U.S. NSF funding EAR-0821631 and EAR-0943407 to PI Kelin Whipple as well as EAR-0922199 to PI Michael Lamb. We thank Leonard Sklar, two anonymous reviewers, AE Dimitri Lague, and Editor Alex Densmore for their thorough reviews.

References

Abbott, J. E., and J. R. D. Francis (1977), Saltation and suspension trajectories of solid grains in a water stream, *Philos. Trans. R. Soc. London, Ser. A*, *284*, 225–254.

Aberle, J., and G.M. Smart (2003), The influence of roughness structure on flow resistance on steep slopes, *J. Hydraul. Res.*, *41*(3). 259–269, doi:10.1080/00221680309499971.

Aguirre-Pe, J., M. L. Olivero, and A. T. Moncada (2003), Particle densimetric froude number for estimating sediment transport, *J. Hydraul. Eng. 129*(6), 428–437, doi:10.1061/(ASCE)0733-9429(2003)129:6(428).

Ancey, C. A., T. Bohm, M. Jodeau, and P. Frey (2006), Statistical description of sediment transport experiments, *Phys. Rev., E 74*, 011302, doi:10.1103/PhysRevE.74.011302.

Ancey, C., A. C. Davison, T. Bohm, M. Jodeau, and P. Frey (2008), Entrainment and motion of coarse particles in a shallow water stream down a steep slope, *J. Fluid Mech.*, *595*, doi:10.1017/S0022112007008774, 83–114.

Bagnold, R. A. (1966), An approach to the sediment transport problem from general physics, *Geol. Surv. Prof.*, Paper 422-t, Washington, D. C.

Bathurst, J. C. (1985), Flow resistance estimation in mountain rivers, *J. Hydraul. Eng.*, *111*, 625–643.

Bathurst, J. C. (1987), Critical conditions for bed material movement in steep, boulder-bed streams, in Erosion and Sedimentation in the Pacific Rim, *Proc. Corvallis Symp., IAHS*, *165*, 309–318.

Browand, F. K., and C. M. Ho (1983), The mixing layer—An example of quasi two-dimensional turbulence, *Journal de Mecanique Theorique et Appliquee Supplement*, Navy-NSF-supported research, 99–120, ISSN:0750-7240.

Buckingham, E. (1915), The principle of similitude, *Nature*, *96*, 396–397.

Buffington, J. M., W. E. Dietrich, and J. W. Kirchner (1992), Friction angle measurements on a naturally formed gravel stream bed: Implications for critical boundary shear stress, *Water Resour. Res.*, *28*, 411–425.

Buffington, J. M., and D. R. Montgomery (1999), Effect of hydraulic roughness on surface textures of gravel-bed rivers, *Water Resour. Res.*, *35*, 3507–3521.

Chatanantavet, P. (2007), Physically-based models of bedrock incision processes in mountain streams, *Ph.D. Dissertation*, University of Minnesota, Minneapolis, 210 pp.

Chatanantavet, P., and G. Parker (2008), Experimental study of bedrock channel alluviation under varied sediment supply and hydraulic conditions, *Water Resour. Res.*, *44*, W12446, doi:10.1029/2007WR006581.

Chatanantavet, P., and G. Parker (2009), Physically based modeling of bedrock incision by abrasion, plucking, and macroabrasion, *J. Geophys. Res.*, *114*, F04018, doi:10.1029/2008JF001044.

Chow, V. T. (1959), Open Channel Hydraulics, 680 pp., McGraw Hill, New York.
Crosby, B. T., K. X. Whipple, and N. M. Gasparini (2007), Formation of fluvial hanging valleys: Theory and simulation, *J. Geophys. Res.*, *112*, F03S10, doi:10.1029/2006JF000566.
Diplas, P., C. L. Dancey, A. O. Celik, M. Valyrakis, K. Greer, and T. Akar (2008), The role of impulse on the initiation of particle movement under turbulent flow conditions, *Science*, *322*, 5902, 717–720, doi:10.1126/science.1158954.
Egashira, S., and K. Ashida (1991), Flow resistance and sediment transportation in streams with step-pool bed morphology, *Lect. Notes Earth Sci.*, *37*, 45–58, doi:10.1007/BFb0011181.
Einstein, H. A. (1950), The bed load function for sediment transportation in open channel flow, *Tech. Bull*. No. 1026, United States Dep. of Agriculture, Washington, D.C. (Sept.)
Ferguson, R. (2010), Time to abandon the Manning equation?, *Earth Surf. Processes Landforms*, *35*, 1873–1876, doi:10.1002/esp.2091.
Ferguson, R. I. (2012), River channel slope, flow resistance, and gravel entrainment thresholds, *Water Resour. Res.*, *48*, W05517, doi:10.1029/2011WR010850.
Fernandez Luque, R., and R. van Beek (1976), Erosion and transport of bed load sediment, *J. Hydraul. Res.*, *14*, 127–144.
Finnegan, N. J., L. S. Sklar, and T. K. Fuller (2007), Interplay of sediment supply, river incision, and channel morphology revealed by the transient evolution of an experimental bedrock channel, *J. Geophys. Res.*, *112*, F03S11, doi:10.1029/2006JF000569.
Francis, J. R. D. (1973), Experiments on the motion of solitary grains along the bed of a water-stream, *Proc. R. Soc. London, Ser. A*, *332*, 443–471.
Gasparini, N. M., R.L. Bras, and K. X. Whipple (2006), Numerical modeling of non–steady-state river profile evolution using a sediment-flux-dependent incision model, in Tectonics, climate, and landscape evolution: *Geol. Soc. of Amer*., Special Paper 398, edited by S. D. Willett, N. Hovius, M. T. Brandon, and D. Fisher, 127–141, doi:10.1130/2006.2398(08).
Gasparini, N. M., K. X. Whipple, and R. L. Bras (2007), Predictions of steady state and transient landscape morphology using sediment-flux-dependent river incision models, *J. Geophys. Res.*, *112*, F03S09, doi:10.1029/2006JF000567.
Gilbert, G. K. (1914), The transportation of debris by running water, *U.S. Geol. Survey Prof. Pap.*, *86*, 263.
Goode, J. R., and E. Wohl (2010), Coarse sediment transport in a bedrock channel with complex bed topography, *Water Resour. Res.*, *46*, W11532, doi:10.1029/2009WR008135.
Hodge, R. A., T. B. Hoey, and L. S. Sklar (2011), Bed load transport in bedrock rivers: The role of sediment cover in grain entrainment, translation, and deposition, *J. Geophys. Res.*, *116*, F04028, doi:10.1029/2011JF002032.
Hu, C., and Y. Hui (1996), Bed-load transport I: Mechanical characteristics, *J. Hydraul. Eng.*, *122*, 245–254.
Johnson, J. P. L., and K. X. Whipple (2007), Feedbacks between erosion and sediment transport in experimental bedrock channels, *Earth Surf. Processes Landforms*, *32*, 1048–1062, doi:10.1002/esp.1471
Johnson, J. P. L., and K. X. Whipple (2010), Evaluating the controls of shear stress, sediment supply, alluvial cover, and channel morphology on experimental bedrock incision rate, *J. Geophys. Res.*, *115*, F02018, doi:10.1029/2009JF001335.
Kamphuis, J. W., (1974), Determination of sand roughness for fixed beds, *J. Hydraul. Res.*, *12*, 193–202.
Keulegan, G. H. (1938), Laws of turbulent flow in open channels, *J. Nat. Bur. Stand.*, Research Paper 1151, *2*, 707–741.
Kirchner, J. W., W. E. Dietrich, F. Iseya, and H. Ikeda (1990), The variability of critical shear stress, friction angle, and grain protrusion in water worked sediments, *Sedimentology*, *37*, 647–672.
Lamb, M. P., W. E. Dietrich, and L. S. Sklar (2008a), A model for fluvial bedrock incision by impacting suspended and bed load sediment. *J. Geophys. Res.*, *113*, F03025, doi:10.1029/2007JF000915.
Lamb, M. P., W. E. Dietrich, and J. G. Venditti (2008b), Is the critical Shields stress for incipient sediment motion dependent on channel-bed slope?, *J. Geophys. Res.*, *113*, F02008, doi:10.1029/2007JF000831.
Lee, H. Y., and I. S. Hsu (1994), Investigation of saltating particle motions, *J. Hydraul. Eng.*, *120*, 831–845.
Montgomery, D. R., and J. M. Buffington (1997), Channel-reach morphology in mountain drainage basins, *Geol. Soc. Am. Bull.*, *109*, 596–611.
Mueller, E. R., J. Pitlick, and J. Nelson (2005), Variation in the reference shields stress for bed load transport in gravel-bed streams and rivers, *Water Resour. Res.*, *41*, W04006, doi:10.1029/2004WR003692.
Neill, C. R. (1968), Note on initial motion of coarse uniform bed material, *J. Hydraul. Res.*, *6*, 173–176.
Nino, Y., M. Garcia, and L. Ayala (1994), Gravel saltation: 1. Experiments, *Water Resour. Res.*, *30*, 1907–1914.
Nitsche, M., D. Rickenmann, J. M. Turowski, A. Badoux, and J. W. Kirchner (2011), Evaluation of bed load transport predictions using flow resistance equations to account for macro-roughness in steep mountain streams, *Water Resour. Res.*, *47*, W08513, doi:10.1029/2011WR010645.
Pagliara, S., and P. Chiavaccini (2006), Flow resistance of rock chutes with protruding boulders, *J. Hydraul. Eng.*, *132*, doi:10.1061/(ASCE)0733-9429(2006)132:6(545).
Parker, G. (2004), 1-D Sediment transport morphodynamics with applications to rivers and turbidity currents, e-book, University of Illinois at Urbana-Champaign, USA, http://hydrolab.illinois.edu/people/parkerg//morphodynamics_e-book.htm
Prancevic, J., M. P. Lamb, and B. Fuller (2012), Relative roughness controls on incipient sediment motion in steep channels, *Eos. Trans*. AGU, Fall meet., EP44B-02.
Recking, A. (2009), Theoretical development on the effects of changing flow hydraulics on incipient bed load motion, *Water Resour. Res.*, *45*, W04401, doi:10.1029/2008WR006826.
Rickenmann, D. and A. Recking (2011), Evaluation of flow resistance in gravel-bed rivers through a large field data set, *Water Resour. Res.*, *47*, W07538, doi:10.1029/2010WR009793.
Schmeeckle, M. W., J. M. Nelson, and J. P. Bennett (2001), Interparticle collision of natural sediment grains in water, *Water Resour. Res.*, *37*, 2377–2391, doi:10.1029/2001WR000531.
Schoklitsch, A. (1962), Handbuch des Wasserbaues, Springer-Verlag, Vienna.
Sekine, M., and H. Kikkawa (1992), Mechanics of saltating grains II, *J. Hydraul. Eng.*, *118*, 536–558.
Shvidchenko, A. B., and G. Pender (2000), Flume study of the effect of relative depth on the incipient motion of coarse uniform sediments, *Water Resour. Res.*, *36*, 619–628.
Shvidchenko, A. B., G. Pender, and T. B. Hoey (2001), Critical shear stress for incipient motion of sand/gravel streambeds, *Water Resour. Res.*, *37*, 2273–2283.
Sklar, L. S., and W. E. Dietrich (2004), A mechanistic model for river incision into bedrock by saltating bed load, *Water Resour. Res.*, *40*, W06301, doi:10.1029/2003WR002496.
Sklar, L. S., and W. E. Dietrich (2006), The role of sediment in controlling steady-state bedrock channel slope: Implications of the saltation–abrasion incision model, *Geomorphology*, *82*, 1–2, doi:10.1016/j.geomorph.2005.08.019.
Tinkler, K. J., and J. Parish (1998), Recent adjustments to the long profile of Cooksville Creek, an urbanized bedrock channel in Ontario, in Rivers Over Rock: Fluvial Processes in Bedrock Channels, Geophys. Monogr. Ser., v. 107, edited by K. J. Tinkler, and E. E. Wohl, pp. 167–187, AGU, Washington, D. C.
Tucker, G. E., and R. Slingerland (1997), Drainage basin responses to climate change, *Water Resour. Res.*, *33*, 2031–2047.
Tucker, G. E., and K. X. Whipple (2002), Topographic outcomes predicted by stream erosion models: Sensitivity analysis and intermodel comparison, *J. Geophys. Res.*, *107*(B9), 2179, doi:10.1029/2001JB000162.
Turowski, J. M., A. Badoux, and D. Rickenmann (2011), Start and end of bed load transport in gravel-bed streams, *Geophys. Res. Lett.*, *38*, L04401, doi:10.1029/2010GL046558.
Turowski, J. M., and D. Rickenmann (2009), Tools and cover effects in bed load transport observations in the Pitzbach, Austria, *Earth Surf. Processes Landforms*, *34*, 26–37, doi:10.1002/esp.1686.
van Rijn, L. C. (1984), Sediment transport, part I: bed load transport, *J. Hydraul. Eng., ASCE*, *110*, 1431–1456.
Whipple, K. X., and G. E. Tucker (2002), Implications of sediment-flux-dependent river incision models for landscape evolution, *J. Geophys. Res.*, *107*(B2), doi:10.1029/2000JB000044.
Wiberg, P. L., and J. D. Smith (1985), A theoretical model for saltating grains in water, *J. Geophys. Res.*, *90*, 7341–7354.
Wohl, E. E., and D. M. Merritt (2001), Bedrock channel morphology, *Geol. Soc. Am. Bull.*, *113*, 1205–1212.
Yager, E. M., J. W. Kirchner, and W. E. Dietrich (2007), Calculating bed load transport in steep boulder bed channels, *Water Resour. Res.*, *43*, W07418, doi:10.1029/2006WR005432.